DEBRIS-CLOUD COLLISION RISK ASSESSMENT WITH GSOC COLLISION AVOIDANCE SYSTEM

A. Trombetta[(1)], A. Zollo[(1)], G. Fasano[(2)], R. Opromolla[(2)], and G. Isoletta[(2)]

[(1)] *German Space Operations Centre (GSOC), DLR, Münchener Str. 20, 82234, Weßling, Germany, email: {annarita.trombetta, andrea.zollo}@dlr.de*
[(2)] *University of Naples "Federico II", Piazzale V. Tecchio 80, 80125 Naples, Italy, email: {g.fasano, roberto.opromolla, giorgio.isoletta}@unina.it*

ABSTRACT

After an in-orbit break-up event, tracking and cataloging fragments takes time, leading to a 'blackout' period where debris is not yet cataloged, and Conjunction Data Messages (CDMs) cannot be issued. Traditional 1-vs-1 collision assessments are ineffective in the short-term phase of debris cloud evolution, which typically lasts some hours after the fragmentation. Additionally, untracked small fragments further increase the risk of undetected impacts on operational spacecraft. In this context, the Flight Dynamics (FD) team at the German Space Operations Center (GSOC) is developing a tool to evaluate the potential collision risk posed by a fragmentation event to their assets, further enhancing the capabilities of their already established Collision Avoidance System (CAS). The proposed methodology is based on a mapping technique that links the position evolution of a primary spacecraft to the Initial Spread Velocity Space (ISVS) at break-up time by recursively solving a series of multi-revolution Lambert's problems. The Probability of Collision (PoC) is then calculated by integrating the Probability Density Function (PDF) of the ejection velocities, as defined by NASA's Standard Break-up Model (SBM), over the volume swept by the primary image in the ISVS. The tool is tested using a benchmark scenario from the literature, with the PoC of a single fragment validated against a Monte Carlo simulation. Specifically, the resulting cumulative risk metric is compared to the one obtained by sampling from the same ejection velocity distribution defined by the SBM and recording any collisions that occur for each sample.

Keywords: break-up, short-term debris cloud evolution, collision risk assessment.

1. INTRODUCTION

With the advancement of space technology, the rate of spacecraft launches has steadily increased, resulting in a growing congestion in Earth's orbital environment. Indeed, over the past decades, this congestion has progressively become more hazardous for spacecraft operations due to a significant rise in space debris. Future projections suggest an even greater surge, driven by the expansion of mega-constellations, which will further contribute to the saturation of the most commonly used orbital regimes. As a result, spacecraft operators are facing a growing number of close encounter alerts and are consistently performing more Collision Avoidance Maneuvers (CAMs) to maintain safety and ensure mission continuity.

Collision avoidance operations are nowadays a vital activity for control centers, where precision and timing are paramount. These operations usually consist of three key stages: conjunction risk assessment, where the severity of a close approach is evaluated; maneuver execution, where a CAM is planned and uploaded to the spacecraft if needed; and post-maneuver recovery, where the spacecraft is restored to its mission configuration after temporarily deviating from its operational orbit. Focusing the attention on the first stage, assessing the criticality of a conjunction event follows a well-established procedure that calculates the Probability of Collision (PoC) and other key metrics of the encounter by considering the states and associated uncertainties of both primary and secondary object [2][4][8][19]. At the German Space Operations Center (GSOC), the Flight Dynamics (FD) team leverages its Collision Avoidance System (CAS) to carefully manage its missions. The CAS relies on Conjunction Data Messages (CDMs) issued by the 19th Space Defense Squadron (19th SDS). Upon receiving a new CDM, the CAS retrieves the latest orbit determination results for the primary object and extracts the secondary object's state vector and covariance data from the CDM. These parameters are then propagated around the Time of Closest Approach (TCA), generating different products that support FD operators in their decision-making process [1].

However, this traditional 1-vs-1 risk assessment approach becomes inadequate in the case of in-orbit break-up events. In fact, immediately following a fragmentation, the encounter between the debris cloud and a target object cannot be treated as a series of individual encounters as the state estimation of each piece of debris may require

Proc. 9th European Conference on Space Debris, Bonn, Germany, 1–4 April 2025, published by the ESA Space Debris Office
Editors: S. Lemmens, T. Flohrer & F. Schmitz, (http://conference.sdo.esoc.esa.int, April 2025)

time. This delay creates a "blackout" period during which satellite operators are unable to take mitigation actions to reduce collision risk. During this time, CDMs cannot be issued. Additionally, very small fragments often go untracked due to technological limitations of current sensors, potentially leading to a dangerous underestimation of the PoC.

Within this context, the GSOC FD team is developing a tool that provides an assessment of the collision risk posed by a fragmentation event to their assets, focusing on the first hours after the break-up.

During this stage, the fragments distribution in true anomaly (ν) is influenced by the value of the parent object. The short-term phase is followed by the medium-term one, where the fragments' ν has already become random and uncoupled from the one of the parent. Finally, in the so-called long-term phase, the fragments' distributions of ascending node (Ω) and argument of perigee (ω) become randomized as well due to the perturbation of $J2$ [6] [7] [11].

Different methodologies have been developed to compute the collision hazard posed by debris clouds to active Resident Space Objects (RSOs). The most straightforward methodologies are based on Monte Carlo simulations. Fragments' ejection velocities are sampled from break-up models and propagated individually [15][23]. Despite their simplicity, these techniques are computationally expensive. Alternative approaches, such as those proposed by [14][16][17], model debris clouds as a continuum. In these methods, key parameters of interest are the debris spatial density and the cloud volume evolution over time. Continuum methods are typically unsuitable for short-term analysis, as they require simplifying assumptions on debris distributions. In the short-term phase in fact, none of the orbital elements distribution is random but still highly time-dependent, leading to significant instability in cloud density. Methods based on Boundary Value Problems (BVPs) are particularly effective for capturing the rapid dynamics of the short-term phase. The research of [12] provides a methodology to pass from the Initial Spread Velocity Space (ISVS) to the physical conjunction space. This is achieved by solving a recursive multi-revolution Lambert's problem to determine the velocity (or velocities) required to reach the targeted position. The recent work of [21] employs a similar approach to estimate impact rates in the absence of orbital perturbations. Further enhancements of this branch of methodologies have been made by [18], estimating the collision risk through high-order Taylor expansions and automatic domain-splitting techniques. Similarly, the work of [20] solves the problem through higher-order BVPs to account for orbital perturbations.

The GSOC tool employs the BVP approach similarly to the implementation in [12], with the key difference being that the collision probability integral is computed in the ISVS. This latter is computed after mapping the primary position evolution to a series of ejection velocities that the fragments at break-up time must acquire in order to hit the primary object at a given time t along its orbit.

The paper is organized as follows. First, in Section 2, an overview of preliminary concepts, including the characterization and evolution of a debris cloud, is presented. The short-term phase is analyzed in detail to better understand the underlying dynamics assumptions and phenomena of interest for the validity of the tool. For completeness, a brief introduction to the medium- and long-term phases is also provided to the interested reader. Subsequently, in Section 3 the methodology is described, including its mathematical details, specific considerations regarding the Lambert problem and the integral formulation to compute the PoC. In Section 5, the methodology is validated through a Monte Carlo simulation reflecting the same initial conditions as the test case provided in Section 4, demonstrating its applicability in real operational conditions. Subsequently, Section 6 gives an overview of the implemented service within the CAS framework, focusing on its product to support decision-making. Lastly, Section 7 provides the conclusions and outlines potential future work.

2. DEBRIS CLOUD CHARACTERIZATION AND EVOLUTION

Fragments resulting from a break-up event of one or more RSOs shall be characterized in terms of their physical and dynamical properties. Immediately before a fragmentation, all future debris is assumed to have the same orbital position as the parent object. However, as shown in Figure 1, after the break-up, each fragment i acquires an additional velocity $\Delta\vec{v}_i$ due to the energy imparted by the explosion or collision. This velocity change can be approximated as impulsive and is added to the parent object's original orbital velocity $\vec{v}_1$. Consequently, each fragment's trajectory changes instantly, and understanding its evolution is crucial for assessing the likelihood of collision with other RSOs. To compute the post break-up state vectors of the fragments, a break-up model has to be involved to quantify the $\Delta\vec{v}_i$.

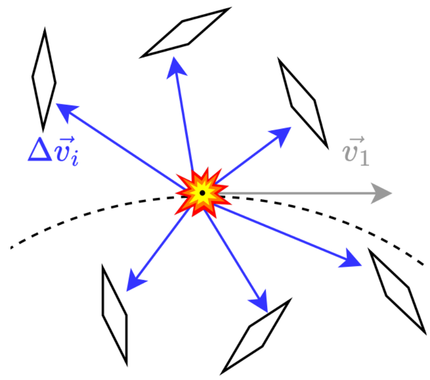

Figure 1: Break-up effect on the fragments' orbital state.

NASA's Standard Break-up Model (SBM) is the most widely used model in debris cloud evolution analysis and collision risk assessment. The SBM describes the outcome of an explosion or collision (both for catastrophic and non-catastrophic events) based on empirical data from ground testing and historical in-orbit fragmentation. However, within the context of this work, we focus exclusively on in-orbit explosions. The model estimates the number of debris generated, along with statistical distributions of their characteristic length, area-to-mass ratio, and, of particular interest for this research, the norm of the ejection velocity [13]. However, the Probability Density Function (PDF) of the ejection velocity magnitudes alone is not sufficient, as the resulting trajectories are also directly influenced by the directions of the $\Delta\vec{v}_i$.

For this work, as in [18], an isotropic direction model has been chosen. The latter is a conservative approach particularly suitable when the break-up physics is not well understood and the ejection geometry is uncertain, since it does not assume a preferred ejection direction. This means that each fragment has an equal probability of being ejected in any direction and the velocity vectors are uniformly distributed over the surface of a sphere [5].

Once the SBM provides the physical and dynamical characteristics of the newly formed cloud, its evolution can be divided into three distinct phases: short-term, medium-term, and long-term evolution.

2.1. Short-term phase

In this stage, the debris cloud initially takes on an ellipsoidal shape, with a high concentration of fragments still clustered around the parent object's original position [6][7][11]. The break-up ejection velocities modify the fragments' orbital periods, gradually spreading them throughout the entire orbit. This process is illustrated in Figure 3, where a two-day simulation depicts the transition from the initial ellipsoidal shape around the parent object to a closed torus around the Earth [22].

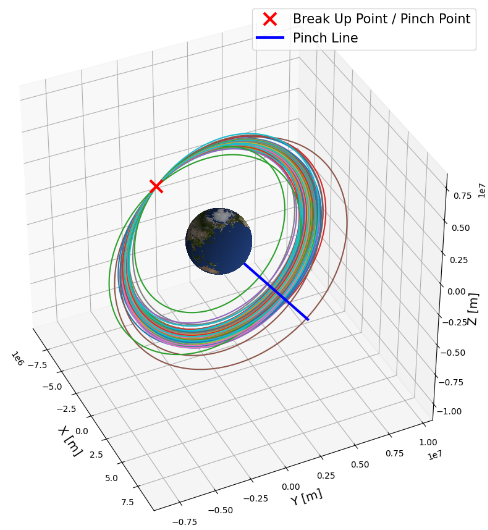

Figure 2: Fragments' orbits forming a pinched torus, with the pinch point at break-up position and the pinch line along the radial direction in the parent orbital plane.

From an orbital mechanics perspective, at the beginning, the distribution of the fragments in true anomaly exhibits only a slight deviation from the parent object's value. Over time, as the imparted velocities take effect and the fragments continue to spread along the orbit, the distribution of ν is gradually randomized. In contrast, the fragments' argument of perigee and right ascension of the ascending node remain biased by their initial value prior to the break-up. This behavior occurs because, at this stage, orbital perturbations are negligible compared to the dominant influence of ejection velocities. This phase typically lasts a few hours and concludes when the ν becomes random, marking the transition of the cloud into a closed torus [6][7][11]. As shown in Figure 2, in the absence of orbital perturbations, the toroid exhibits a so-called pinch point at the original break-up location. This point represents a region where numerous fragments pass through almost simultaneously as a result of their localized sudden change in orbital velocity. Around the pinch point, the local cloud density is temporarily much higher than in other regions of the cloud. Similarly, a pinch line forms along the radial direction in the parent orbit plane, located at exactly 180° from the pinch point, as all debris must also pass through the orbital plane along this line [5]. Additionally, the internal motion of the cloud causes the formation of pinch sheets, where a significant fraction of the debris cloud aligns temporarily, forming elongated high-density regions [12].

Without the influence of orbital perturbations, the cloud would indefinitely retain its pinched toroidal shape. In reality, perturbative forces are present and begin to significantly influence the cloud's dynamics in the medium- and long-term phases [6][7][11]. As demonstrated in [22], the role of the $J2$ perturbation in the short-term phase is negligible, as the only orbital parameter that changes is the mean anomaly, driven by the varying orbital energies of the fragments. Therefore, the motion of the fragments during this phase can be assumed to be purely Keplerian, justifying the use of a debris cloud collision risk assessment tool that neglects perturbations, as the objective is to focus on short-term dynamics.

2.2. Medium and long-term phases

The medium-term phase begins immediately after the formation of the closed torus and is entirely governed by the $J2$ perturbation [6][7][11]. The Earth's oblateness introduces two primary secular effects on the fragments dynamics. Firstly, it induces a precession of ω, causing the apsidal line of the debris orbits to rotate within their respective orbital planes. Secondly, it leads to a precession of Ω, occurring at a slower rate compared to the one of ω. Consequently, the distributions in ω and in Ω begin to spread, gradually moving toward randomization. The toroid slowly dismantles and transforms into a band surrounding the Earth, whose latitude is limited by the inclination of the parent orbit [6][7][11]. This phase typically lasts from several months to several years, with its exact duration strongly influenced by the initial conditions of the break-up event. The transition from the medium-term to the long-term phase, during which a toroidal structure

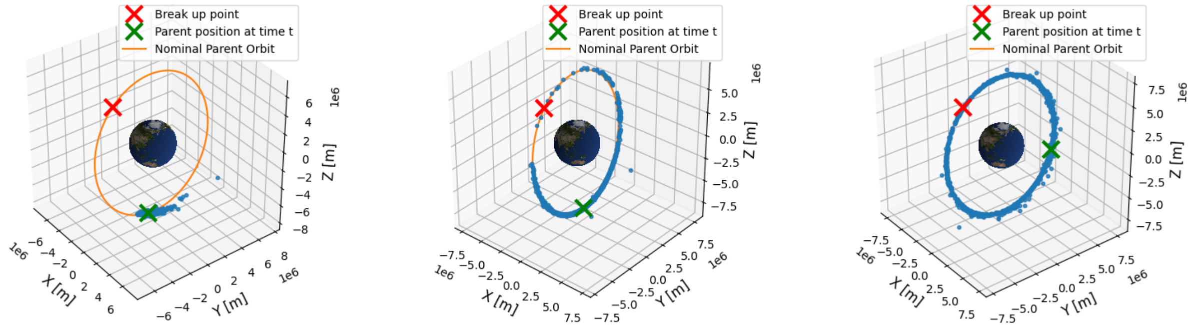

Debris cloud after 1 hour   Debris cloud after 12 hours   Debris cloud after 2 days

Figure 3: Short-term evolution: transition from ellipsoidal shape phase to complete randomization of fragments' true anomaly (closed torus formation).

evolves into a debris band, is neither instantaneous nor abrupt. Instead, it is a slow, gradual process that can take several years. To account for this progression, an intermediate "bridge" phase is often considered. During this period, differential nodal precession rates gradually begin to open the toroidal structure at the equator while maintaining higher debris density at high latitudes due to the persistence of pinch zones [6][11]. Finally, the last phase starts where the predominant perturbation is the atmospheric drag. Its effect gradually reduces the density of the debris cloud over time [6][7][11].

3. METHODOLOGY

This section provides a comprehensive analysis of how to calculate the PoC between a primary object and a cloud of fragments. It is important to note that all the figures presented in this section are intended as visual support for the analytical treatment but refer to a specific test case discussed in Section 4.

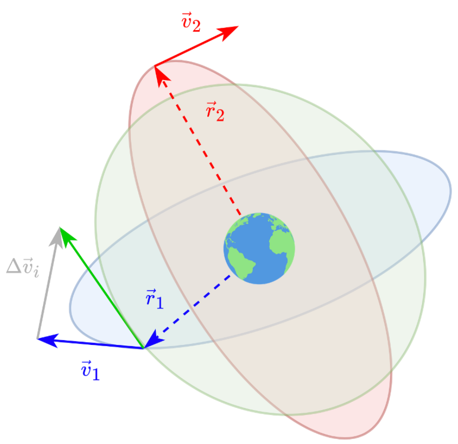

Figure 4: Geometrical illustration of the initial conditions with break-up of a parent object at $\vec{r_1}$ and primary position $\vec{r_2}$ at break-up time t_0.

Following the illustration in Figure 4, consider the explosion of an RSO, referred to as the parent object, occurring at position $\vec{r_1}$ at time t_0 (break-up time), while traveling with an orbital velocity $\vec{v_1}$. Each fragment i of the resulting cloud acquires an additional velocity $\Delta\vec{v_i}$, leading to a new orbital velocity:

$$\vec{v_i}(t_0) = \vec{v_1} + \Delta\vec{v_i}, \quad \forall i = 1, ..., N \tag{1}$$

where N is the total number of generated fragments. Now, consider a primary object at time t_0 with position $\vec{r_2}$, moving with velocity $\vec{v_2}$. Following the approach outlined in [12], we define the simulation time T such that the assumptions of short-term phase hold and we discretize the time-window $[t_0, T]$ into a series of time instances t_j. At each time node, the primary position $\vec{r_2}(t_j)$ is mapped to the corresponding $\Delta\vec{v_j}$ a fragment would have at t_0 to hit the primary at time t_j. This is done by recursively solving a Lambert problem $L(*)$ considering the initial position of the fragments at t_0 and the position of the primary at each time node [10].

$$\Delta\vec{v_j} = L_j(\vec{r_1}(t_0),\ \vec{r_2}(t_j),\ t_j - t_0), \quad \forall j \in [t_0, T] \tag{2}$$

where $t_j - t_0$ indicates the time of flight of the transfer and the velocity increments $\Delta\vec{v_j}$ are defined relative to the initial parent orbital velocity $\vec{v_1}$.
As the primary advances along its orbit, in the physical space, the Lambert problem solutions $\Delta\vec{v_j}$ trace trajectories in the space of the ejection velocities at t_0. These trajectories are depicted in Figure 6 where each point corresponds to a $\Delta\vec{v}$ vector that would cause a collision at a future time t_j. This space is referred to as the ISVS.
For a specific time of flight, Lambert's solver provides multiple solutions depending on the number of revolutions of the transfer orbit. This implies that distinct $\Delta\vec{v_j}$ may co-exist for the same value of the time of flight. Therefore, all these solutions must be taken into account in the subsequent mathematical treatment of the PoC computation.
Figure 5 depicts the Lambert transfer orbits for a fixed number of revolutions M. As it can be seen, the trajectories start from the break-up position (blue cross) and end

in the primary location at various points along its orbit. The transfers are color-coded to indicate the magnitude of the required $\Delta\vec{v_j}$ for transitioning from the parent orbit onto these trajectories. Darker colors correspond to lower ejection velocity values.

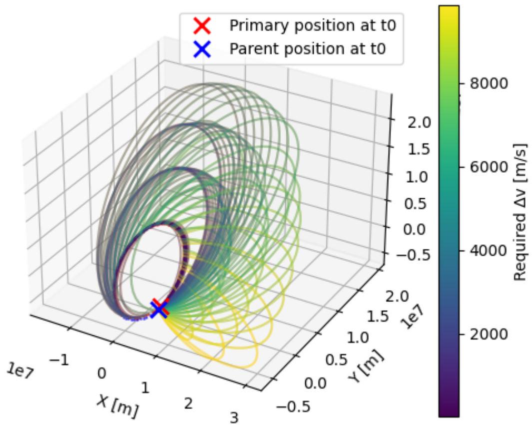

Figure 5: Lambert's transfers for a number of revolutions $M = 0$. The Δv magnitudes of the plotted orbits are color-coded in the vertical bar on the right. For improved graphical clarity, only solutions with $\Delta v < 10000\ m/s$ are shown.

In general, shorter flight times require higher ejection velocities to reach the corresponding primary position. The reader is encouraged to observe, in Figure 5, the presence of multiple shells of transfer orbits. Each shell corresponds to a specific set of time of flights, grouping together successive valid Lambert solutions. Additionally, each of these groups is linked to a specific piecewise segment of the primary path in the ISVS, shown in Figure 6. This can be understood by examining two consecutive formulations of the Lambert problem, namely L_j and L_{j+1}. Their respective solutions $\Delta\vec{v_j}$ and $\Delta\vec{v_{j+1}}$ are not necessarily adjacent in the ISVS due to constraints imposed by the BVP geometry.

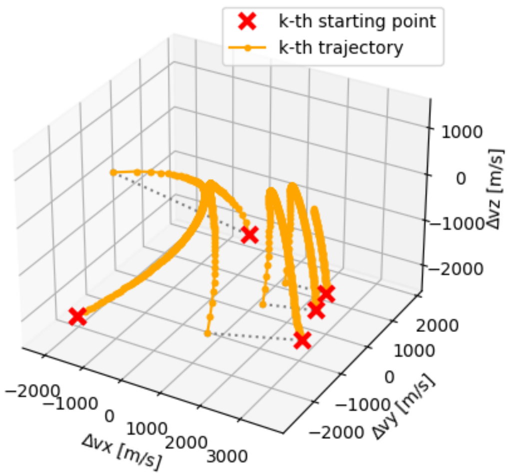

Figure 6: Piecewise trajectory of the primary object in the ISVS for a number of revolutions $M = 0$.

Once the role of the BVP approach has been clarified, we can now introduce the formulation for computing the probability P_i that only a single fragment collides with the primary. By definition of PDF, the probability that a realization of the random vector $\Delta\vec{v}$ falls within the subset ζ, representing all $\Delta\vec{v_i}$ leading to a collision at a future time t_j, is given by integrating the ejection velocity PDF $f(\Delta\vec{v})$ over the volume swept by the primary's image in the ISVS, as expressed in Equation 3.

$$P_i = \int_{\zeta} f(\Delta\vec{v})\,\mathrm{d}V \tag{3}$$

Where, $f(\Delta\vec{v})$ can be represented as:

$$f(\Delta\vec{v}) = \frac{f(\log_{10}\Delta v)}{4\pi\Delta v^2[\Delta v\ln(10)]} \tag{4}$$

In this expression, $f(\log_{10}\Delta v)$ represents the distribution of ejection velocity magnitudes, following a normal distribution with a mean of $\mu = 2.63$ and a standard deviation of $\sigma = 0.48$. This formulation was developed by [9] and employed in [21], and it is based on the original SBM distribution, with the key simplification of removing the dependency on the area-to-mass ratio. To obtain the corresponding $f(\Delta\vec{v})$, we assume that the ejection velocities are uniformly distributed over a sphere as mentioned in Section 2.
The integration volume $\mathrm{d}V$ can be then expressed as:

$$\mathrm{d}V = A\left\|\frac{\mathrm{d}\Delta\vec{v}}{\mathrm{d}t}\right\|\mathrm{d}t \tag{5}$$

where A is the collision cross-section of the primary in the ISVS, whose normal is parallel to the time derivative of the $\Delta\vec{v}$. The latter should not be interpreted as a physical acceleration but rather as the first derivative of the curves in the ISVS given by BVP solutions. Consequently, the product of its norm and $\mathrm{d}t$ represents a positional displacement in the ISVS. By substituting Equation 5 into Equation 3, the expression for P_i becomes:

$$P_i = \sum_k \int_{T_k} f(\Delta\vec{v_k})A_k\left\|\frac{\mathrm{d}\Delta\vec{v_k}}{\mathrm{d}t}\right\|\mathrm{d}t \tag{6}$$

The summation over the segments k indicates an integration over the piecewise curves in the ISVS, accounting for the presence of multiple possible paths over a sufficiently long propagation window.
The PoC of the entire debris cloud corresponds to the probability that at least one fragment out of the total N will collide with the primary within the given time window. The latter is computed using fundamental principles of probability theory, assuming that collisions of different fragments are stochastically independent events. It is given by:

$$PoC = 1 - (1 - P_i)^N \tag{7}$$

It is worth remarking that Keplerian dynamics has been employed as perturbative effects on the cloud evolution are negligible within the first few hours of simulations. The presented formulation inherently accounts for uncertainties in the ejection velocity by incorporating the PDF derived from the SBM. However, uncertainties in the positions of both the parent and the primary object are neglected. This simplification is justified by the fact that the SBM PDF introduces significant uncertainties that dominate any inaccuracies in the initial position of the parent or the state of the primary, effectively masking their influence.

3.1. Mapping the primary object into the ISVS

In a classical 1-vs-1 conjunction scenario, the dimensions of both colliding objects must be considered. However, in this specific case, the size of the fragments can be neglected, as the majority are significantly smaller than the target object. Additionally, the exact size of a debris fragment cannot be determined at this early stage, as no information from the catalog is available. For simplicity, the primary object is assumed to be a sphere of radius R in the physical space. Unlike the approach of [12], the integral for computing the PoC is performed in the ISVS. Consequently, the dimensionality of the primary must be mapped accordingly.
The primary sphere can be transformed from the physical space to the ISVS through the linear map $\mathbf{\Phi}_{3\times3}(t_j)$, representing the 3 by 3 sub-part of the 6 by 6 state transition matrix, which links the velocity at time t_0 to the position at time t_j. The primary image in the final space takes the form of an ellipsoid as indicated by Equation 8 and represented in Figure 7.

$$\Delta\vec{v_j}^T \mathbf{\Phi}_{3\times3}^T(t_j)\mathbf{\Phi}_{3\times3}(t_j)\Delta\vec{v_j} = R^2 \tag{8}$$

The collision cross-section in the ISVS at time t_j is given by the area of the transformed ellipsoid projected onto the plane whose normal, illustrated as a blue vector in Figure 7, is defined by the direction of the time derivative of $\Delta\vec{v}$. As it can be seen, ellipsoids tend to shrink secularly over time, resulting in a reduction of the primary cross-section area in the ISVS.

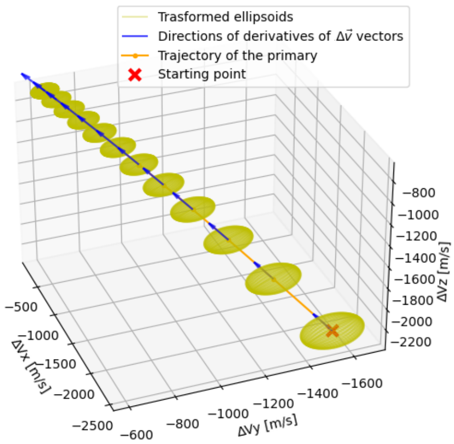

Figure 7: Primary sphere mapped into ellipsoids in the ISVS at different time instants t_j.

As a consequence, the integration volume becomes thinner. A physical interpretation for this is that, as the debris cloud evolves, its density decreases, resulting, on average, in a lower flux of fragments passing through the primary sphere [12].

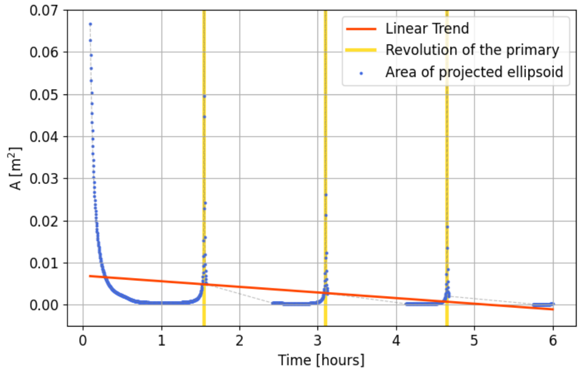

Figure 8: Time evolution of projected ellipsoids areas A with a linear decrease over the simulation time T for a number of revolutions $M = 0$.

Figure 8 illustrates the evolution of A over the simulation time. The collision cross-section exhibits a periodic pattern: during one revolution of the primary object, as it approaches the pinch region, A tends to locally increase up to a singularity. Conversely, when the primary moves away from this region, the cross-section shrinks. This local oscillation of A does not contradict the fact that the cloud density is decreasing, as mentioned above. In fact, when considering a longer time scale, A is decreasing on average, as confirmed by the least squares linear regression performed on the data points in red. Such singularities should be filtered out, since they are introducing numerical errors and do not provide a faithful representation of the actual physics involved.

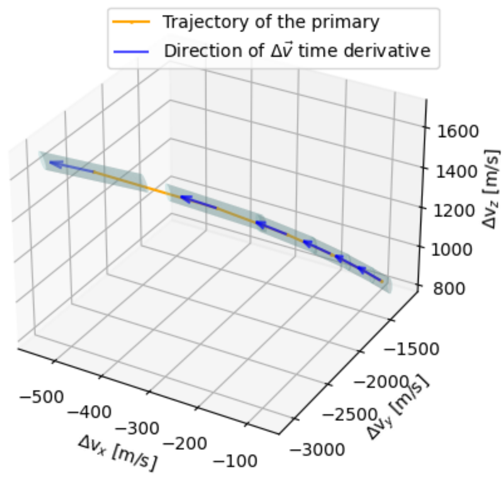

Figure 9: Integration volume over a portion of the primary path in the ISVS for a number of revolutions $M = 0$.

As defined in Equation 5, the integration volume ultimately takes the form of a tube with an elliptical section around the primary's trajectory in the ISVS. A portion of this volume is shown in Figure 9. Since the integration is performed numerically, certain regions may be subject to under- or over-estimation, depending on how the trajectory bends. Specifically, there may be portions of the path where two consecutive differential volumes overlap, leading to a local over-accumulation of PoC, or regions where gaps exist between consecutive volumes, causing some parts to be entirely omitted.

4. TEST CASE

To verify the described methodology, the new capability of the GSOC CAS has been tested for a high-PoC scenario in LEO environment. The same test case employed by [18] and [21] has been selected. It simulates the explosion of a 900 kg generic parent object, causing a debris cloud of 2.2×10^6 fragments larger than 1 mm. The target object is assumed to be the International Space Station (ISS) and the conjunction risk is computed within a time window of 6 hours following the fragmentation event. Without loss of generality, the ISS is approximated to a spherical target of 50 m radius, despite its actual dimensions, to represent a typical asset on a LEO orbit. Table 1 summarizes the initial condition of both parent and primary at time t_0.

Table 1: Orbital parameters for ISS and parent object at break-up time.

Parameter	ISS	Parent
a [km]	6800	7000
e	1.8000×10^{-4}	2.6970×10^{-2}
i [°]	51.60	50
Ω [°]	0	0
ω [°]	359.9973	180
ν [°]	307.7498	139.6759

For this specific scenario, certain Lambert's solutions have been filtered out. The preliminary conjunction assessment presented in [18] suggests considering only solutions with $\Delta\vec{v}$ magnitude larger than a maximum threshold of $\Delta v_{max} = 3890$ m/s. This accounts for 95% of the fragments. The filtering process is advantageous as it helps reduce computational time without causing significant underestimation of the PoC. This is because extremely large Δv values correspond to low PDF values, and thus contribute negligibly to the overall integral.
The series of Lambert's solutions in Figure 5 generates the trajectories in ISVS depicted in Figure 6. The integration is then performed as described in Section 3 producing the cumulative PoC against the simulation time illustrated in Figure 10. This plot considers the risk posed by the entire cloud, namely the quantity described in Equation 7, exhibiting good agreement with results published in [18] and [21]. With a red horizontal line, we represent the typical GSOC risk mitigation threshold. The cumulative PoC reaches a final value of 0.01760 after 6 hours of simulation. Notably, a rapid accumulation is observed during the first 30 minutes, in contrast to the following hours, where the PoC gradually stabilizes and approaches a steady state. Clearly, this represents an artificial high-probability scenario that is unlikely to occur frequently in real space operations, which explains why the maneuver threshold is exceeded so quickly. The plot has been retrieved by including at each t_j the contribution to the instantaneous PoC of all available BVP solutions for different values of M. Ordering all solutions at each time step is essential to ensure a consistent instantaneous impact rate and accurately reflect the physics of the problem.

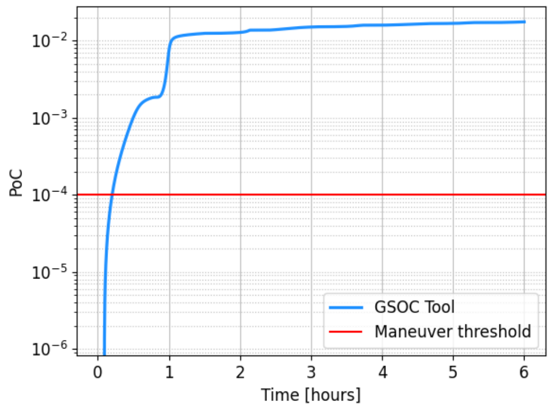

Figure 10: Debris cloud cumulative collision probability for the test case presented in Table 1.

5. MONTE CARLO VALIDATION

The results of Section 4 are validated by computing the PoC of a single fragment through a Monte Carlo simulation. Considering the contribution of only one fragment is sufficient as it is directly linked to the PoC generated by the entire cloud through Equation 7. The Monte Carlo validation has been performed by sampling the same ejection velocity distribution described by Equation 4. Each sample and the primary have been propagated into the future using Keplerian dynamics, in accordance with the validity assumptions of the methodology. For each sample, a discrete grid of miss distances has been computed and subsequently interpolated using a cubic spline. The final Monte Carlo PoC was then calculated as the ratio between the number of samples resulting in a hit and the total number of samples.
The PoC of a single fragment colliding with the primary is naturally lower than the PoC generated by the entire cloud, which would require a significantly larger number of samples, leading to extensive computational time. To mitigate this, the primary object's diameter was artificially increased to 100 km. A total of 5×10^5 samples were used to produce the results in Figure 12. The outcome of the Monte Carlo simulation is compared to the PoC computed by the GSOC tool under the same condi-

tions, i.e., a 100 km diameter and one fragment, as represented by the blue line. The tool effectively captures the PoC trend, reaching a final error of 0.7%. In detail, a larger discrepancy between the two curves occurs at the initial stages of the simulation. This is due to the presence of samples with $\Delta v > \Delta v_{max}$, which are inherently included in the Monte Carlo simulation and, instead, filtered out by the tool. Approximately 2.5% of the samples exceeded this threshold.
It is worth mentioning that in some parts of the graph, the two curves do not match perfectly, as the GSOC software does not exactly align with the Monte Carlo reference.

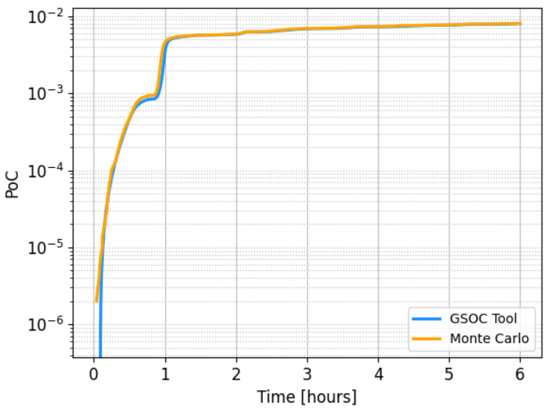

Figure 12: Comparison between cumulative PoC computed by the GSOC tool and Monte Carlo reference. The validation refers to the PoC produced by a single fragment and for a spherical target of 100 km diameter.

This discrepancy arises from the intrinsic numerical nature of the methodology, which integrates by summing a discrete series of cylinders, as described in Section 3. As mentioned, when the curvatures of the trajectories in the ISVS increase, the PoC can be wrongly over- or under-estimated. Despite this, the integration error balances out over the course of the simulation, allowing the final Monte Carlo PoC to be reached with an acceptable tolerance.

6. CAS DEBRIS CLOUD COLLISION RISK ASSESSMENT ROUTINE

The following section provides a brief explanation of how the tool integrates into the operational framework of the CAS. Designed as a supporting functionality, it aids in analyzing and managing operations when a break-up event occurs. This capability is seamlessly integrated into the CAS, as illustrated in Figure 11. In this prototype version, the user provides an estimate of the break-up epoch, a time window of interest T, a propagation timestep Δt for the primary evolution, and the physical properties and state vector of the parent object at the moment of break-up. This data is then passed to the SBM, as it is essential for generating the number of fragments produced by the explosion. Subsequently, the software computes the Δv magnitude distribution and the empirical PDF in Equation 4. Subsequently, the CAS retrieves the latest orbit determination results for the primary object and propagates it with the time-step defined by the user. The software then produces a plot of the time evolution of the PoC, as in Figure 10, where the maneuver threshold is given as an indicator of the event's criticality. In the unlikely case that the PoC exceeds the predefined maneuver threshold, this serves as an indication that further, more detailed analyses should be initiated to properly assess potential mitigation actions. Although additional output, such as the solutions to Lambert's problem and the representation of primary trajectories in the ISVS, are not strictly necessary from an operational standpoint, they can also be consulted by the operator to better understand

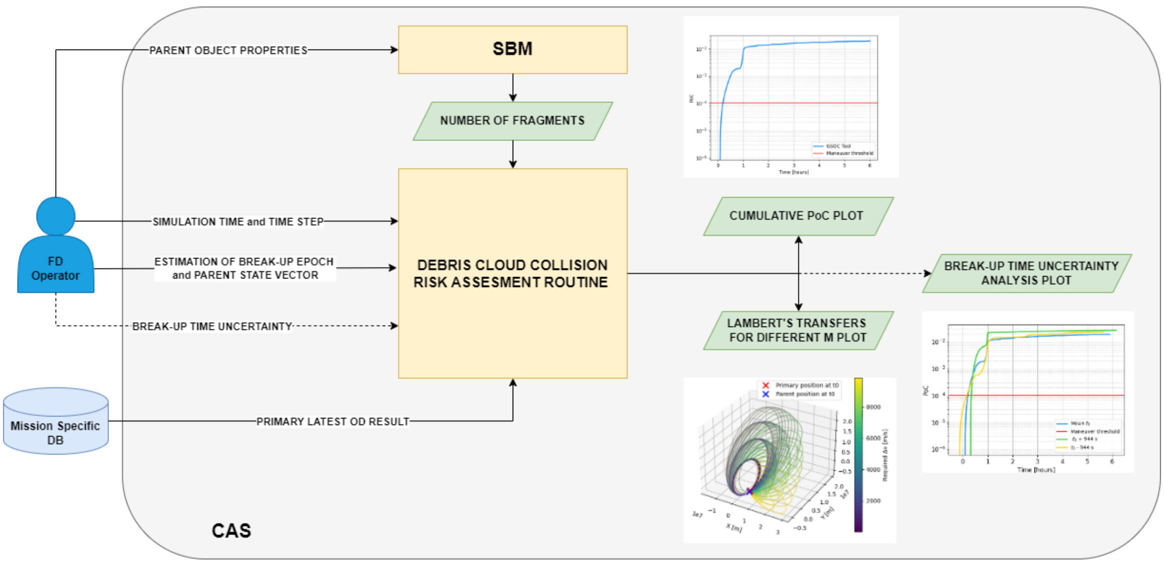

Figure 11: Workflow description of the debris cloud collision risk assessment routine integrated into the CAS.

the underlying physics of the event.
The software also offers the possibility to rerun the simulation accounting for the uncertainty related to the break-up epoch. The determination of the latter is a complex process and is affected by different sources of uncertainties. As a result, predicting the exact time of an in-orbit break-up is practically impossible, especially in the few hours following the event. To account for this, the user can provide a standard deviation σ_t, which is used by the tool to recalculate the initial conditions at the updated time $t_{new} = t_0 \pm \sigma_t$. At this point the analysis is repeated with different initial conditions for both parent and primary objects. Specifically, their mean anomaly M is updated by means of the Kepler's equation. Finally, the tool displays the cumulative PoC evolution based on the original t_0, and also provides PoC curves for $t_{new} = t_0 \pm \sigma_t$. Figure 13 shows the result of the test case in Table 1, shifting the break-up epoch by $\pm 944\ s$ in time [24]. The plot illustrates how the PoC curves are affected by this time shift, since the relative geometry of the problem has changed. The case that exceeds the threshold first will be the main driver for initiating potential mitigation actions.

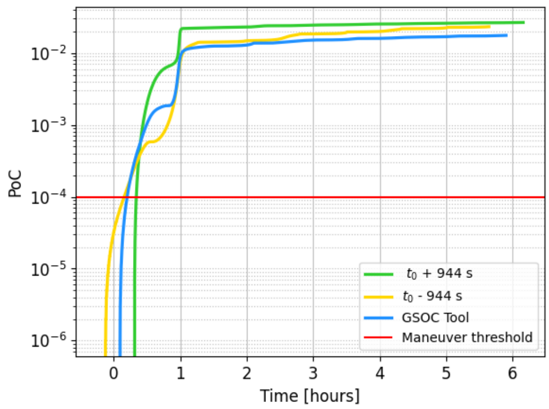

Figure 13: PoC curves corresponding to different break-up times for the test case presented in Table 1.

7. CONCLUSIONS AND FUTURE WORK

This paper has presented the new feature of the GSOC CAS developed by the FD team for assessing short-term collision risk posed by debris clouds following in-orbit explosions. By employing a BVP approach and a mapping technique to the ISVS, the tool effectively computes the PoC, capturing the complex evolution of a debris cloud in the short-term phase. The methodology has been validated against a Monte Carlo simulation for a high-probability scenario, reaching an accuracy of the final PoC value of about 0.7%. The operational framework in which the tool is developed is also described, with a focus on its input, output and potential supporting plots to the operators.
As future work, the FD team is planning to extend the applicability of the software to a cloud generated by in-orbit collisions. If such an event occurs, fragments belong to two distinct parents, with two different orbital velocities. To address this, fragments must be linked to a specific parent in order to obtain their initial orbital velocity. This can be done in various ways, either by using a statistical approach or a more physically consistent method that ensures the conservation of physical laws, such as momentum conservation. After this process, the short-term probability of collision can be computed following the same methodology presented in this work. Another improvement for the current version of the software is to tackle the over- and under-estimation by employing geometrical workarounds, such as the one described by [3]. Another interesting line of research is to enhance the methodology to include the primary positional uncertainty in the formulation.

REFERENCES

1. Aida S., (2016). Conjunction Risk Assessment and Avoidance Maneuver Planning Tools, *6th International Conference on Astrodynamics Tools and Techniques.*
2. Alfano S., (2005). A Numerical Implementation of Spherical Object Collision Probability, *Journal of the Astronautical Sciences*, **53**, 103-109.
3. Alfano S., (2008). Beta conjunction analysis tool, *Advances in the Astronautical Sciences*, **129**, 2245-2256.
4. Alfriend K. T., Akella M. R., Frisbee J., et al., (1999). Probability of Collision Error Analysis, *Space Debris*, **1**, 21-35.
5. Barrows S., (1996). Evolution Of Artificial Space Debris Clouds, *University Of Southampton, Department of Aeronautics and Astronautics, Doctoral Thesis.*
6. Barrows S. P., Swinerd G. G., and Crowther R., (1996). Review of Debris-Cloud modeling techniques, *Journal of Spacecraft and Rockets*, **33**(4), 550–555.
7. Chobotov A., Spencer D. B., Schmitt D. L., et al., (1988). Dynamics of Debris Motion and the Collision Hazard to Spacecraft Resulting From an Orbital Breakup, *Aerospace Corp. TR SD-TR-88-96.*
8. Foster J. A., Estes H. S., (1992). Parametric analysis of orbital debris collision probability and maneuver rate for space vehicles, *NASA JSC, Technical Report.*
9. Frey S., Colombo C. (2021). Transformation of satellite breakup distribution for probabilistic orbital collision hazard analysis, *Journal of Guidance, Control, and Dynamics*, **44**, 88–105.
10. Izzo D., (2015). Revisiting Lambert's problem, *Celestial Mechanics and Dynamical Astronomy*, **121**(1), 1-15.
11. Jehn R. (1990). Dispersion of Debris Cloud from In-Orbit Fragmentation Events, *Dresden International Astronautical Federation Congress*.
12. Jenkin A. B., (1996). Probability of Collision During the Early Evolution of Debris Clouds, *Acta Astronautica*, **38**(4), 525–538.

13. Johnson N. L., Krisko P. H., Lieu J.-C., et al., (2001). Pergamon NASA'S NEW BREAKUP MODEL OF EVOLVE 4.0., *Adv. Space Res.*, **28**, 1377-1384.

14. Letizia F., Colombo C., and Lewis H. G., (2015). Analytical Model for the Propagation of Small-Debris-Object Clouds after Fragmentations, *Journal of Guidance, Control, and Dynamics*, **38**(8), 1478–1491.

15. Liou J.-C., Hall D., Krisk, P., et al., (2004). LEGEND — A Three-Dimensional LEO-to-GEO Debris Evolutionary Model, *Advances in Space Research*, **34**(5), 981–986.

16. McInnes C., (1993). An Analytical Model for the Catastrophic Production of Orbital Debris, *ESA Journal*, **17**(4), 293–305.

17. Nazarenko A., (1997). The Development of the Statistical Theory of a Satellite Ensemble Motion and Its Application to Space Debris Modeling, *Second European Conference on Space Debris.*

18. Parigini C., Algethamie R., and Armellin R., (2024). Short-Term Collision Probability Caused by Debris Cloud, *Journal of Guidance, Control, and Dynamics*, **47**(5), 1–13.

19. Patera R., (2001). General Method for Calculating Satellite Collision Probability, *Journal of Guidance Control and Dynamics*, **24**(4), 716-722.

20. Shu P., Yang Z., Luo Y.-z., and Sun Z.-J., Collision Probability of Debris Clouds Based on Higher-Order Boundary Value Probems, *Journal of Guidance, Control, and Dynamics*, **45**(8), 1–11.

21. Shu P., Yang Z., and Luo Y.-Z., Impact Risk of a Debris Cloud to Spacecraft, *Journal of Guidance, Control, and Dynamics*, **46**(5), 989–997.

22. Trombetta A., (2024). Analysis of In-Orbit Break-Up Models, Debris Cloud Evolution, and Short-term Collision Risk Assessment, *University of Naples "Federico II", Master Thesis*

23. Walker R., Martin C., Stokes P., et al., (2001). Analysis of the Effectiveness of Space Debris Mitigation Measures Using the Delta Model, *Advances in Space Research*, **28**(9), 1437–1445.

24. Wang R., Feng S., et al., (2024). Breakup analysis of Cosmos 1408 Satellite, *Journal of Space Safety Engineering*, **11**(2), 335-341.